Image restoration and segmentation using the Ambrosio-Tortorelli functional and discrete calculus

Marion Foare, Jacques-Olivier Lachaud
Laboratoire de Mathématiques
Université Savoie Mont-Blanc
Email: {marion.foare,jacques-olivier.lachaud}@univ-savoie.fr

Hugues Talbot
Laboratoire d'Informatique Gaspard-Monge
Université Paris-Est – ESIEE
Email: hugues.talbot@univ-paris-est.fr

***Abstract*—Essential image processing and analysis tasks, such as image segmentation, simplification and denoising, can be conducted in a unified way by minimizing the Mumford-Shah (MS) functional. Although seductive, this minimization is in practice difficult because it requires to jointly define a sharp set of contours and a smooth version of the initial image. For this reason, various relaxations of the original formulations have been proposed, together with optimisation methods. Among these, the Ambrosio-Tortorelli (AT) parametric functional is of particular interest, because minimizers of AT can be shown to converge to a minimizer of MS. However this convergence is difficult to achieve numerically using standard finite difference schemes. Indeed, with AT, discontinuities need to be represented explicitly rather than implicitly. In this work, we propose to formulate AT using the full framework of Discrete Calculus (DC), which is able to sharply represent discontinuities thanks to a more sophisticated topological framework. We present our proposed formulation, its resolution, and results on synthetic and real images. We show that we are indeed able to represent sharp discontinuities and as a result significantly better stability to noise, compared with finite difference schemes.**

Keywords: segmentation, denoising, simplification, Mumford-Shah functional, variational formulation, optimisation, inverse problems.

I. Introduction

We are interested in some essential tasks of image processing and image analysis, particularly image segmentation, image restoration and image cartooning. For these tasks, the Mumford-Shah (MS) functional [1] has emerged as a very powerful formulation, seeking to represent an image with a piecewise smooth approximation. This approximation can be viewed as a denoising and simplication process, and the frontiers of the smooth pieces can be interpreted as a segmentation. In practice, however, the MS functional is difficult to optimize due to the joint simplification and contour delineation that it requires. Despite that difficulty, MS has served as an inspiration to many very well known and widely used methods, such as the Rudin-Osher-Fatemi (ROF) restoration method, TV denoising, or the Chan-Vese and Boykov-Jolly segmentation methods, and many others. The original formulation of MS is in the continuous domain but purely discrete versions have also been proposed (Graph Cuts). After recalling the MS functional, we present a new digital formulation of the Ambrosio-Tortorelli (AT) functional, an accurate approximation of MS that converges toward it.

A. The Mumford-Shah functional

Given an input grayscale image defined in an open bounded domain of $\mathbb{R}^2$, we represent its gray levels by a function $g \in L^\infty(\Omega)$. In the Mumford-Shah (MS) model, one wants to find a pair (K, u), where the compact set $K \in \bar{\Omega}$ represents the discontinuities of g and the function $u \in W^{1,2}(\Omega \backslash K)$ is a smooth reconstruction of g except on K. The pair (K, u) is found by minimizing the Mumford-Shah functional [1]

$$\mathcal{MS}(K,u) = \alpha \int_{\Omega\backslash K} |u-g|^2 \ \mathrm{dx} + \int_{\Omega\backslash K} |\nabla u|^2 \ \mathrm{dx} + \lambda\, \mathcal{H}^1(K \cap \Omega) \quad (1)$$

where $\alpha, \lambda > 0$ and $\mathcal{H}^1$ denotes the 1-dimensional Haussdorff measure. The first term forces the approximation u to be close to the original image g, while the second one constrains u to be smooth and the last one penalizes the length of the set of discontinuities K.

But the minimisation of (1) depends on a pair (K, u) of a priori independent objects. Hence, we work with a relaxed version of the MS functional (1) ([2]), defined for a function $u \in \mathrm{SBV}(\Omega)$ by

$$MS(u) = \alpha \int_{\Omega} |u-g|^2 \ \mathrm{dx} + \int_{\Omega} |\nabla u|^2 \ \mathrm{dx} + \lambda\, \mathcal{H}^1(\mathcal{J}_u) \quad (2)$$

where $\mathcal{J}_u$ denotes the set of jumps of u, *i.e.* the set of discontinuities of u. This relaxed functional depends solely on u and we want to minimize it in the class of special functions of bounded variation in Ω. Unfortunately the minimization is still delicate due to the computation of the 1-dimensional Haussdorff measure. We therefore turn to another formulation.

B. The Ambrosio-Tortorelli functional formulation

The Ambrosio-Tortorelli (AT) functional [3] is defined by

$$\mathrm{AT}_\varepsilon(u,v) = \int_\Omega \alpha|u-g|^2 + v^2|\nabla u|^2 + \lambda\varepsilon|\nabla v|^2 + \frac{\lambda}{4\varepsilon}|1-v|^2 \ \mathrm{dx}, \quad (3)$$

for functions $u, v \in W^{1,2}(\Omega)$ with $0 \le v \le 1$.

In (3), u denotes a smooth approximation of the input image g while v is a smooth approximation of $(1 - \chi_{\mathcal{J}_u})$. Ambrosio and Tortorelli proved in [3] that their functional (3) Γ-converges to the MS functional (2) as ε tends to 0.

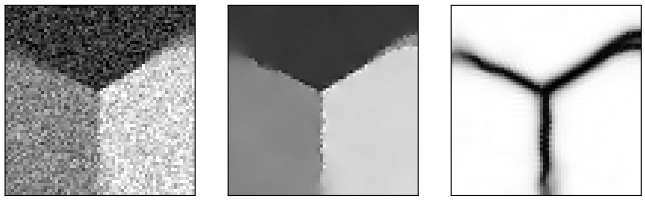

input g u v

Figure 1: Minimizing AT with finite differences on a triple point with noise 0.2. The resulting thickness of $v \sim 6$px implies poor denoising on the contours of u.

Intuitively, a large ε induces a solution with a fuzzy set of discontinuities, which is then progressively narrowed to the crisp 1-dimensional set of discontinuites as ε goes to 0.

This notion of convergence ensures that if we can compute a sequence $(u_\varepsilon)_\varepsilon$ of minimizers of AT, and if u_ε converges to some function $u \in \mathrm{SBV}(\Omega)$, then u is a minimizer of the Mumford-Shah functional. For more details about Γ-convergence and AT, we refer the reader to [4] and [5].

Unfortunately, the minimization of (3) with standard discretization schemes such as finite differences or finite elements leads to difficulties. Chambolle and Bourdin [6] point out that for convergence, parameters ε, the gridstep h and the ratio $\frac{\varepsilon}{h}$ must all tend to zero. In practice this is unfeasible, and ε is set to approximately $5h$. This implies that the set $\{v \approx 0\}$ is thick, as we can see in Fig. 1. An alternative method, proposed in [6], is to refine the meshing of the domain locally around the set of discontinuities of u.

C. Related works

Many works derive from the study of the Mumford-Shah functional, which can be seen both as a segmentation and a restoration model. The MS functional is non-convex and difficult to optimize, so most contributions propose workable relaxations. On the restoration side, in [7], authors propose an effective simplification resulting into a piecewise-constant model for image denoising. In [8], an exact solution of the Total Variation (TV) regularisation term using convex analysis is proposed. Various implementations are freely available [9], [10], [11]. On the segmentation side, the most common simplification is the Chan-Vese model [12], which uses level sets. In practice it is limited to a binary output. A convex formulation is proposed in [13]. Approximate discrete methods have also been proposed, for instance using Graph Cuts [14] or parametric contour selection on hierarchical segmentation representation, for instance [15], [16].

The Ambrosio-Tortorelli relaxation for both restoration and segmentation was studied and discretized with a finite-differences scheme in [17]. As we shown on Fig. 1, this leads to a thick approximation of v and poor convergence properties as $\varepsilon \to 0$. To correct this, authors in [6] use finite elements, and an adaptive mesh that is realigned and refined around discontinuities. Kee and Kim [18] proposed several convex relaxations of AT functional, by using the factorability of some non-convex problems. Their best relaxation leads to blurry edges, as well as some false contours. Recently [19] proposed a piecewise smooth segmentation method that is a convex relaxation of MS using Fenchel duality, but this relaxation is sensitive to noise. Recently an AT-based formulation for tubular structure segmentation was proposed in [20], using finite differences.

Finally authors in [21] studied regularization terms similar to AT, and [22] studied their convergence, with implications to our problem.

D. Contributions and Outline

We therefore propose a new approach to the resolution of AT. We discretize it in the framework of discrete calculus. This framework can encode differential forms of different dimensions by relating them to cells of different dimensions. The key ingredient of our digital formulation is that we define v to live in-between u. Intuitively, since discontinuities are supposed to have null Hausdorff-2 measure, this is exactly where discontinuities should be defined. They are thus in-between smooth parts which have non null Hausdorff-2 measure. In Section II, we present the standard discrete calculus operators and two digital formulations of AT functional. Then in Section III we evaluate experimentally our digital AT models for both restoration and segmentation of gray-level and color images, and compare them with standard approaches. Finally, we discuss, conclude and propose future works in Section IV.

II. Digital Ambrosio-Tortorelli functional

A. Discrete exterior calculus

We want to optimize (3). Since standard numerical schemes are not really adapted to this optimization, we propose to reformulate it in the setting of discrete exterior calculus (DEC), as described in the context of computer graphics in [23] and image analysis in [24]. The rationale for this is the greater degree of control over the topology of the problem that this approach allows. The image domain is decomposed into a 2-dimensional cubical complex K, composed of vertices, edges, and faces (see Fig. 2). adjacent vertices. We denote by $\mathbf{d}_k$ and $\bar{\mathbf{d}}_k$ the standard discrete exterior primal and dual derivative operators. Given a $k-$form, the hodge star operator $\star$ returns the corresponding $2-k$ form. We define $\mathbf{M}_{01}$ the matrix which transforms a 0-form into a 1-form by averaging the values on the two edge extremities, i.e. $\mathbf{M}_{01} = \frac{1}{2}|\mathbf{d}_0|$. Moreover, we use the edge laplacian defined in [24] by $\bar{\star}\bar{\mathbf{d}}_0\star\mathbf{d}_1 + \mathbf{d}_0\bar{\star}\bar{\mathbf{d}}_1\star$.

B. Discrete formulations of AT

We first set u and g to live on the faces and v to live on the vertices and edges. Functions u and g are 2-forms since they represent the gray levels of each pixel. Since v is an estimation of the set of discontinuities of u, it should be of null Haussdorff-1 measure. This implies v should be set in-between cells of non null measure, so in this case on edges or vertices. In the following formulation, we set v solely on the vertices, i.e. it is a 0-form. We call this formulation $\mathrm{AT}_\varepsilon^{2,0}$. In

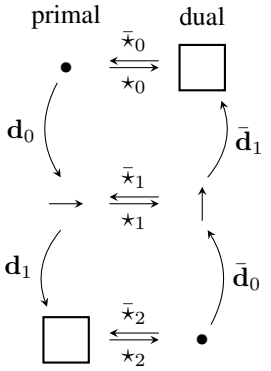

Figure 2: DEC operators

this instance the only difficulty lies in the second, cross term of (3), since its components do not live on the same elements. Hence we use matrix $\mathbf{M}_{01}$ to transport the 0-form v onto edges by simple averaging, yielding (4):

$$\begin{aligned}\mathrm{AT}_\varepsilon^{2,0}(u,v) =&\alpha\langle u-g,u-g\rangle_2 + \langle \mathbf{M}_{01}v,\bar{\star}\bar{\mathbf{d}}_0\star u\rangle_1^2 \\ &+ \lambda\varepsilon\langle \mathbf{d}_0 v,\mathbf{d}_0 v\rangle_1 + \frac{\lambda}{4\varepsilon}\langle 1-v,1-v\rangle_0. \quad (4)\end{aligned}$$

A second possibility is to define u and g on the vertices and v on the edges. We denote this formulation $\mathrm{AT}_\varepsilon^{0,1}$. Contrary to the previous formulation, the gray levels are seen as point mass on the center of pixels, so that functions u and g are both 0-forms. An alternative interpretation is to say that pixels are dual 2-forms, while v is a dual 1-form in between u. This yields (5):

$$\begin{aligned}\mathrm{AT}_\varepsilon^{0,1}(u,v) =&\alpha\langle u-g,u-g\rangle_0 + \langle v,\mathbf{d}_0 u\rangle_1\langle v,\mathbf{d}_0 u\rangle_1 \\ &+ \lambda\varepsilon\langle(\mathbf{d}_1+\bar{\star}\bar{\mathbf{d}}_1\star)v,(\mathbf{d}_1+\bar{\star}\bar{\mathbf{d}}_1\star)v\rangle_1 \\ &+ \frac{\lambda}{4\varepsilon}\langle 1-v,1-v\rangle_1. \quad (5)\end{aligned}$$

We further extend (4) and (5) to the vectorial case by associating to each component of the input image n forms $\{g_1,\ldots,g_n\}$, and the corresponding forms $\{u_1,\ldots,u_n\}$, and summing over the coordinates. In this paper, we will use $n=1$ for gray-level images and $n=3$ for RGB color images.

C. Optimization process

In both cases, the functionals $\mathrm{AT}_\varepsilon^{2,0}$ and $\mathrm{AT}_\varepsilon^{0,1}$ are sums of quadratic terms. They are independently, but not simultaneously, convex in u and v. They must have null derivative at optimum. We thus propose to alternatively solve for u, then v. The derivatives can be given explicitly as linear systems:

$$\begin{cases} \left[\alpha\mathbf{Id} - \mathbf{B}'^{\intercal}\mathrm{diag}\left(\mathbf{M}_{01}v\right)^2\mathbf{B}'\right] u=\alpha g, \\ \left[\frac{\lambda}{4\varepsilon}\mathbf{Id} + \lambda\varepsilon\mathbf{A}^\intercal\mathbf{A} + \mathbf{M}_{01}{}^\intercal\mathrm{diag}\left(\mathbf{B}'u\right)^2)\mathbf{M}_{01}\right] v=\frac{\lambda}{4\varepsilon}\mathbf{1}. \end{cases} \quad (6)$$

for the derivative of $\mathrm{AT}_\varepsilon^{2,0}$, and

$$\begin{cases} \left[\alpha\mathbf{Id} - \mathbf{A}^\intercal\mathrm{diag}\left(v\right)^2\mathbf{A}\right] u=\alpha g, \\ \left[\frac{\lambda}{4\varepsilon}\mathbf{Id} + \lambda\varepsilon(\mathbf{A}'^{\intercal}\mathbf{A}' + \mathbf{B}^\intercal\mathbf{B}) + \mathrm{diag}\left(\mathbf{A}u\right)^2\right] v=\frac{\lambda}{4\varepsilon}\mathbf{1}. \end{cases} \quad (7)$$

for the derivative of $\mathrm{AT}_\varepsilon^{0,1}$. Here $\mathbf{A}$, $\mathbf{B}$, $\mathbf{A}'$ and $\mathbf{B}'$ are the matrices corresponding to the respective operators $\mathbf{d}_0$, $\mathbf{d}_1$, $\bar{\star}\bar{\mathbf{d}}_1\star$ and $\bar{\star}\bar{\mathbf{d}}_0\star$. Otherwise said, $\mathbf{A}$ is the vertex to edge incidence matrix, $\mathbf{B}$ the edge to face incidence matrix, and $\mathbf{A}'$ and $\mathbf{B}'$ their respective transpose (except on image boundary). All matrices are symmetric, definite and positive, so we use a Cholesky factorization to solve alternatively the two equations of (6) (resp. (7)). Because of the $\mathbf{Id}$ additive term, the left-hand is full rank, yielding a unique minimum at each iteration. It is a known result in convex analysis linked to block coordinate descent algorithms [25, Prop. 2.7.1], that these iterations must converge to a stationary point of $\mathrm{AT}_\varepsilon^{2,0}$ (resp.$\mathrm{AT}_\varepsilon^{0,1}$).

III. Numerical experiments

A. Results

We now present numerical results obtained by minimizing the two digital formulations of the AT functional given by (4) and (5) for gray-level and color images. We overlay in red the set of discontinuities, which is defined to be either the set of edges where the two adjacent 0-forms v are less than $\frac{1}{2}$ in (4), or when the 1-form v is less than $\frac{1}{2}$ in (5). For reference to the parameters, all images are normalized to $[0,1]$.

1) Scale-space: In the optimization process, we can introduce a scale-space on the parameter λ. For fixed α, λ constrains the discontinuities total length. Hence, for a large enough λ none are present, so that the minimization of AT is equivalent to a diffusion. We can then choose α for an inital blur on the input data. Then, by decreasing λ, we capture more and more contours, as illustrated in Fig. 3.

2) Joint restoration and contour detection: In the second column of Fig. 4, we illustrate the restoration and segmentation of the noisy triple point presented in Fig. 1, using our digital formulations of AT. We can clearly see that v is no longer thick and diffuse but matches the set of discontinuities of u very well. This is due to the fact that decreasing ε progressively in the optimization process. In the beginning, a large ε allows us to localize approximately the set of discontinuities. As ε decreases to 0, v becomes increasingly precise. In our formulation, at the optimum v can truly be 1-dimensional, lying in between pixel in both our digital formulations given by (4) and (5). Indeed v is defined on null measure forms and cannot vanish on them.

This particularity in our approach allows us to restore images with texture or very thin structures, as illustrated on the Barbara or mandrill pictures presented in Fig. 5 and Fig. 6 respectively.

The previous argument also explains the robustness to noise of our approach, illustrated in Fig. 4 on the image of the triple point with increasing levels of additive Gaussian noise, up to very high levels with $\sigma = 0.8$.

B. Comparisons

In Fig. 7, we compare our approach to some state of the art methods using TV convex relaxations of the MS functional [10], [11]. We also compare to the recent work of Strekalovskyi and Cremers [19], which also considers the AT

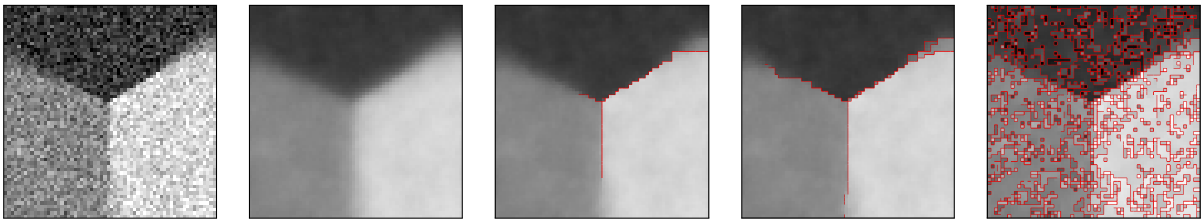

Figure 3: Illustration of the λ-scale-space with $AT_\varepsilon^{0,1}$, Gaussian noise $\sigma = 0.2$, $\varepsilon \in [1, 0.25]$, $\alpha = 0.162$

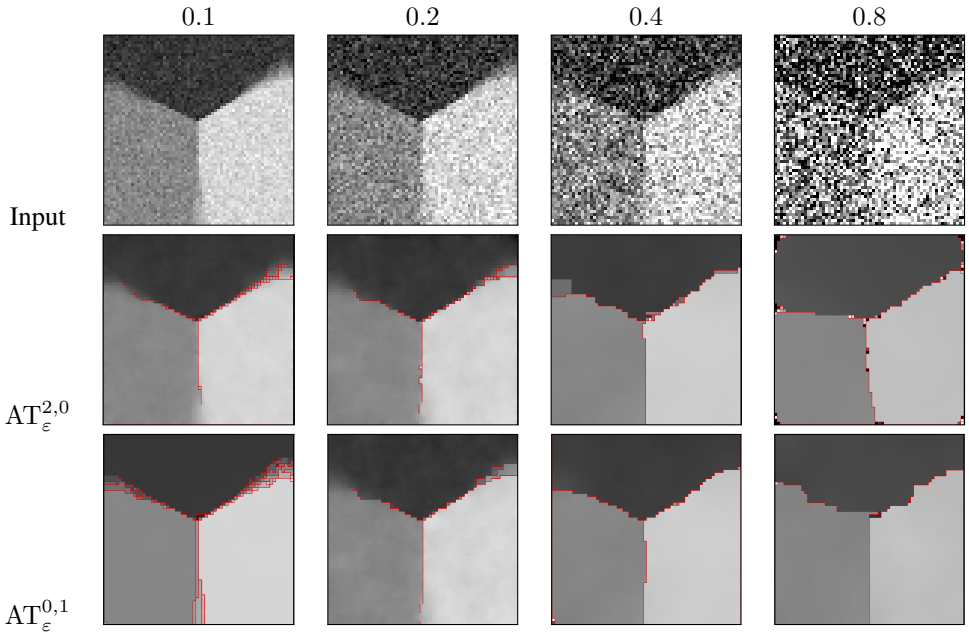

Figure 4: Behaviour of our algorithm for both formulation, with increased levels of noise. For all figures $\varepsilon \in [1, 0.25]$ parameters for $\mathrm{AT}_\varepsilon^{2,0}$, resp. $\lambda = (0.0058, 0.0058, 0.0028, 0.0008)$ and $\alpha = (0.279, 0.135, 0.0126, 0.0032)$ $\mathrm{AT}_\varepsilon^{0,1}$: resp. $\lambda = (0.0001, 0.0048, 0.0005, 0.001)$ and $\alpha = (0.018, 0.1615, 0.0126, 0.0087)$

Figure 5: Input corrupted with Gaussian noise $\sigma = 0.1$ (first column), restoration (second column), contours with $\mathrm{AT}_\varepsilon^{0,1}$, $\lambda = 0.0054088$ and $\alpha = 1.0$; contours with $\mathrm{AT}_\varepsilon^{2,0}$, $\lambda = 0.0064905$ and $\alpha = 0.69$. For both, $\varepsilon \in [1, 0.25]$

functional. The TV relaxations of MS do not produce contours, so we focus on the restoration results. For a fair comparison, for all methods, we set the parameters that maximize the PSNR. Specifically:

- TV denoising using the Chambolle algorithm [11] : we have to guess σ the standard deviation of additive Gaussian noise and λ is the parameter in front of the fidelity term. In the experiments, λ is dynamically computed and we found $\sigma = 21$ for the mandrill and $\sigma = 23$ for the Lena image.
- ROF TV denoising using split Bregman [10], parameters are the same as above.

Strekalovskyi and Cremers propose in [19] to directly minimize the MS functional using a non-convex primal-dual algorithm depending on two parameters α and λ : the first controls the smoothing term while the thresholding parameter λ forces a discontinuity when $\alpha|\nabla u|^2 > \lambda$. We optimized the parameters via grid search.

Figure 6: Restoration results on color images. Parameters: $\varepsilon \in [1, 0.25]$
$\mathrm{AT}_\varepsilon^{2,0}$: resp. $\lambda = (0.0649, 0.0376)$ and $\alpha = (0.833, 0.469)$ $\mathrm{AT}_\varepsilon^{0,1}$: resp. $\lambda = (0.0376, 0.0217)$ and $\alpha = (0.833, 0.48)$

Table I: Best PSNRs results are in bold.

	Barbara	Mandrill	Lena
TV, Getreuer [10]	29.69992	24.94800	29.35474
TV, Duran *et. al.* [11]	29.78958	24.96413	**29.35980**
Strekalovskyi *et. al.* [19]	29.17148	24.14088	28.46289
$\mathrm{AT}_\varepsilon^{2,0}$	29.86778	**25.99681**	28.91914
$\mathrm{AT}_\varepsilon^{0,1}$	**29.91011**	25.04922	29.03297

C. Implementation details

The tools used in this work will be made available in the open-source DGtal library [26], which provides optimized implementations of discrete exterior calculus operators. For the Barbara picture (348x271) presented in Fig. 5, each inner loop iteration takes approximatively 10 seconds and 30 seconds when minimizing respectively (4) and (5). Optimization of AT functional needs on average 5 iterations at any given ε.

IV. Conclusion

We have presented a novel algorithm for optimizing the non-convex Ambrosio-Tortorelli functional, itself a high-quality formulation of the full piecewise-smooth Mumford-Shah functional. Using discrete calculus implementations, we have been able to specify true 1D contour, set in between pixels, ensuring sharp contours and smooth regions. Our algorithms are robust to noise and provide good quality restoration, as evidenced in table I. Future work will involve improving speed, introducing anisotropy in the framework, and work on non-image data such as point clouds or mesh restoration.

References

[1] D. Mumford and J. Shah, "Optimal approximations by piecewise smooth functions and associated variational problems," *Communications on pure and applied mathematics*, vol. 42, no. 5, pp. 577–685, 1989.

[2] E. De Giorgi, M. Carriero, and A. Leaci, "Existence theorem for a minimum problem with free discontinuity set," 1989.

[3] L. Ambrosio and V. M. Tortorelli, "Approximation of functional depending on jumps by elliptic functional via t-convergence," *Communications on Pure and Applied Mathematics*, vol. 43, no. 8, pp. 999–1036, 1990.

[4] G. Buttazzo, "γ-convergence and its applications to some problem in the calculus of variations," *School on Homogenization, ICTP, Trieste*, vol. 1994, pp. 38–61, 1993.

[5] A. Braides, *Approximation of Free-Discontinuity Problems*. Lecture Notes in Mathematics, Vol. 1694, Springer-Verlag, pp. 89–91, 1998.

[6] B. Bourdin and A. Chambolle, "Implementation of an adaptive finite-element approximation of the mumford-shah functional," *Numerische Mathematik*, vol. 85, no. 4, pp. 609–646, 2000.

[7] L. I. Rudin, S. Osher, and E. Fatemi, "Nonlinear total variation based noise removal algorithms," *Physica D: Nonlinear Phenomena*, vol. 60, no. 1, pp. 259–268, 1992.

[8] A. Chambolle, "An algorithm for total variation minimization and applications," *Journal of Mathematical imaging and vision*, vol. 20, no. 1-2, pp. 89–97, 2004.

[9] J. Duran, M. Moeller, C. Sbert, and D. Cremers, "Collaborative total variation: A general framework for vectorial tv models," *arXiv preprint arXiv:1508.01308*, 2015.

[10] P. Getreuer, "Rudin-osher-fatemi total variation denoising using split bregman," *Image Processing On Line*, vol. 2, pp. 74–95, 2012.

[11] J. Duran, B. Coll, and C. Sbert, "Chambolle's projection algorithm for total variation denoising," *Image Processing On Line*, vol. 2013, pp. 311–331, 2013.

[12] T. F. Chan and L. A. Vese, "Active contours without edges," *Image processing, IEEE transactions on*, vol. 10, no. 2, pp. 266–277, 2001.

[13] M. Nikolova, S. Esedoglu, and T. F. Chan, "Algorithms for finding global minimizers of image segmentation and denoising models," *SIAM J. Appl. Math*, vol. 66, no. 5, pp. 1632–1648, 2006. [Online]. Available: http://dx.doi.org/10.1137/040615286

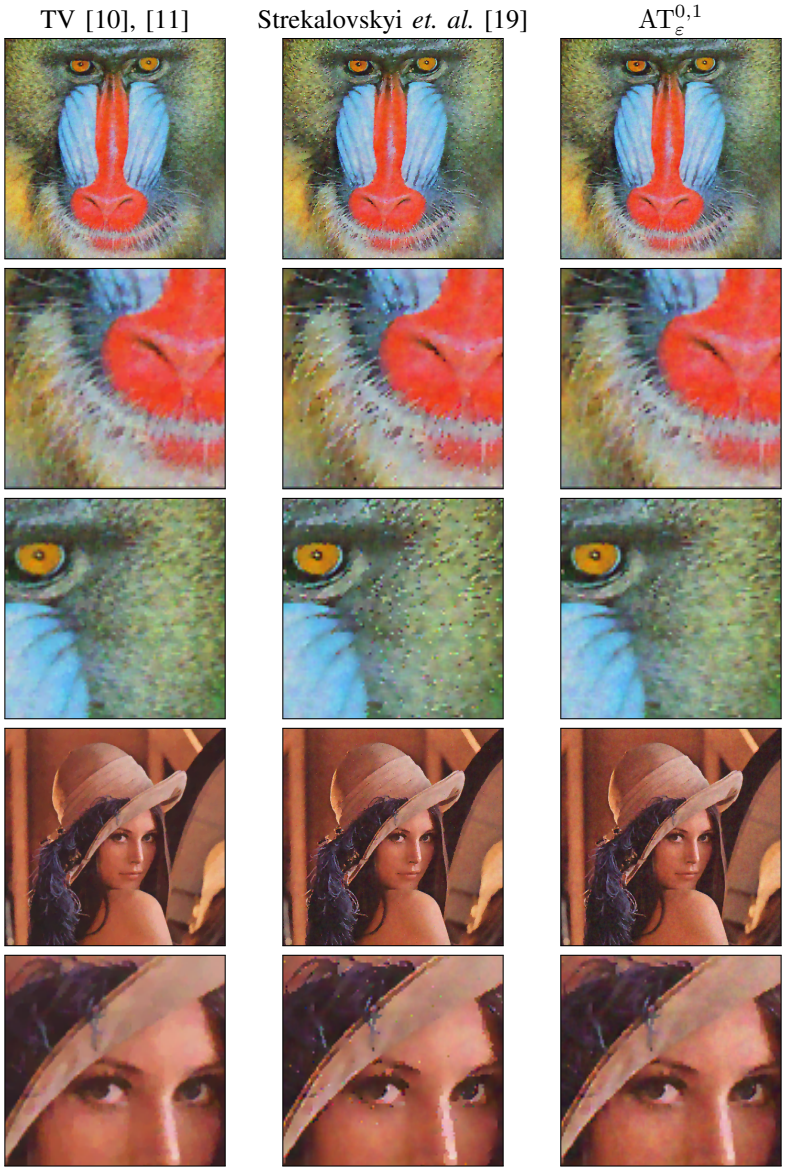

Figure 7: Comparison with competing methods. We observe the characteristic staircasing effect with the TV methods. Strekalovskyi *et. al.* retains a lot of noise. Our method is robust to noise, retains details and yield a piecewise smooth result.

[14] Y. Boykov and G. Funka-Lea, "Graph cuts and efficient nd image segmentation," *International journal of computer vision*, vol. 70, no. 2, pp. 109–131, 2006.

[15] L. Grady and C. V. Alvino, "The piecewise smooth mumford–shah functional on an arbitrary graph," *Image Processing, IEEE Transactions on*, vol. 18, no. 11, pp. 2547–2561, 2009.

[16] L. Guigues, J. Cocquerez, and H. Le Men, "Scale-sets image analysis," *International Journal of Computer Vision*, vol. 68, no. 3, pp. 289–317, 2006.

[17] L. Vese and T. F. Chan, *Reduced non-convex functional approximations for image restoration & segmentation*. Department of Mathematics, University of California, Los Angeles, 1997.

[18] Y. Kee and J. Kim, "A convex relaxation of the ambrosio–tortorelli elliptic functionals for the mumford-shah functional," in *Proceedings of the IEEE Conference on Computer Vision and Pattern Recognition*, 2014, pp. 4074–4081.

[19] E. Strekalovskiy and D. Cremers, "Real-time minimization of the piecewise smooth mumford-shah functional," in *Computer Vision–ECCV 2014*. Springer, 2014, pp. 127–141.

[20] D. Vicente, "Mumford-Shah model for detection of thin structures in an image," Theses, Universite d'Orleans, Sep. 2015. [Online]. Available: https://hal.archives-ouvertes.fr/tel-01231219

[21] P. Charbonnier, L. Blanc-Féraud, G. Aubert, and M. Barlaud, "Deterministic edge-preserving regularization in computed imaging," *Image Processing, IEEE Transactions on*, vol. 6, no. 2, pp. 298–311, 1997.

[22] J. Idier, "Convex half-quadratic criteria and interacting auxiliary variables for image restoration," *Image Processing, IEEE Transactions on*, vol. 10, no. 7, pp. 1001–1009, 2001.

[23] M. Desbrun, A. N. Hirani, M. Leok, and J. E. Marsden, "Discrete exterior calculus," *arXiv preprint math/0508341*, 2005.

[24] L. J. Grady and J. Polimeni, *Discrete calculus: Applied analysis on graphs for computational science*. Springer, 2010.

[25] D. P. Bertsekas, *Nonlinear programming*, 2nd ed. Athena scientific, 1999.

[26] DGTAL: Digital Geometry tools and algorithms library, "http://dgtal.org."